Study of dense helium plasma in the optimal hypernetted chain approximation

H.-M. Müller and K. Langanke
W. K. Kellogg Radiation Laboratory, 106-38, California Institute of Technology, Pasadena, California 91125
(Received 15 April 1993)

We have studied the helium plasma in the hypernetted chain approximation considering both short-ranged internuclear and long-ranged Coulomb interactions. The optimal two-particle wave function has been determined in fourth order; fifth-order corrections have been considered in the calculation of the two-body and three-body correlation functions. The latter has been used to determine the pycnonuclear triple-alpha-fusion rate in the density regime 10^8 g/cm^3 $\leq \rho \leq 10^{10}$ g/cm^3, which is of importance for the crust evolution of an accreting old neutron star. The influence of three-particle terms in the many-body wave function on the rate is estimated within an additional variational hypernetted chain calculation. Our results support the idea that the helium liquid undergoes a phase transition to stable ^{8}Be matter at densities $\rho \approx 3 \times 10^9$ g/cm^3 as the plasma induced screening potential then becomes strong enough to bind the ^{8}Be ground state.

PACS number(s): 21.30.+y, 67.20.+k, 97.60.−s

I. INTRODUCTION

There was recently some interest in the fusion of three α particles (triple-α reaction) in a dense helium plasma. This interest was motivated by a starquake model, based on the crust evolution of an accreting, old neutron star, which has been proposed to explain the frequently observed γ-ray bursts [1]. The energy eventually released in this starquake model turned out to be rather sensitive to the triple-α rate. As has been pointed out by Schramm *et al.* [2], helium forms a quantum fluid under the conditions governing the evolving neutron star crust, a fact which had not been accounted for in the estimates of the triple-α rate [3,4] available at the time the starquake model was proposed. Schramm *et al.* argued that the hypernetted chain approximation (HNC) is a proper method to describe the helium plasma under the relevant conditions (low temperatures $T < 10^6$ K and high densities $\rho_9 \approx 0.1 - 1.0$, where ρ_9 measures the density in 10^9 g/cm^3). These authors performed a variational HNC calculation describing the helium plasma by a Jastrow-like many-body wave function:

$$\Psi(\{\mathbf{r}_i\}) = \prod_{i<j} f(|\mathbf{r}_i - \mathbf{r}_j|) = \prod_{i<j} f(r_{ij}) \ , \qquad (1)$$

where $\mathbf{r}_i$ are the position vectors of the helium nuclei in the plasma, which is assumed to be homogeneous and isotropic. For the two-body wave function $f(r_{ij})$, Schramm *et al.* made a parametrized ansatz which correctly described the known behavior of the function at small and large separations. The parameters invoked in $f(r)$ were determined by minimizing the energy of the system adopting the HNC approximation to connect $f(r)$ with the two-body correlation function $g^{(2)}(r)$. Knowing $g^{(2)}(r)$, Schramm *et al.* applied the Kirkwood approximation to determine the three-body correlation function $g^{(3)}(r)$,

$$g^{(3)}(r_{12}, r_{13}, r_{23}) = g^{(2)}(r_{12}) g^{(2)}(r_{13}) g^{(2)}(r_{23}) \ , \qquad (2)$$

which allowed them to calculate the triple-α rate in the plasma which is defined as [2]

$$r_{3\alpha} = \frac{1}{6} \rho^3 g^{(3)}(r_{13} \approx 0, r_{23} \approx 0) V_r^2 \Gamma_\gamma(E_{3\alpha}) \ . \qquad (3)$$

Here, ρ is the α-particle number density, V_r is the reaction volume, and the radiative decay width of the 3α state at energy $E_{3\alpha}$ can be expressed in terms of the experimentally known Γ_γ width of the first exited 0^+ state in ^{12}C ($\Gamma_\gamma = 3.7$ MeV) for $E2$ decay into the 2^+ state at 4.44 MeV. At energies just above the 3α threshold, one finds $\Gamma_\gamma(E_{3\alpha}) \approx 0.54 \Gamma_\gamma$, independently of $E_{3\alpha}$.

The approach of Schramm *et al.* has recently been improved in two important ways [5].

(1) The optimal wave function $f_0(r)$ has been determined in a lowest-order ($n = 0$) HNC approximation.

(2) For this optimal wave function, the two-body correlation function has been calculated in higher-order HNC approximations ($n = 4, 5$). This allowed one to derive the three-body correlation function taking corrections beyond the simple Kirkwood approximation (2) into account.

As an interesting result, this calculation [5,6] supported the idea [2] that the helium plasma undergoes a phase transition to stable ^{8}Be matter at densities around $\rho_9 = 3$ as then the ^{8}Be ground state gets bound in the medium. However, the critical density of this phase transition depends sensitively on the plasma-induced screening potential which had only been calculated in lowest HNC order in Refs. [5,6]. To improve on this, we will in this paper determine the optimal wave function $f(r)$ and, relatedly, the plasma-induced screening potential, in a HNC/4 approximation. To our knowledge, our study presents the first optimal higher-order HNC solution to a quantum plasma taking both short-ranged nuclear and long-ranged Coulomb interactions into account.

A second motivation of our study is to improve the estimate of the triple-α rate, as given in our previous calculation [5]. As we will see below, this rate will have

 ©1994 The American Physical Society

essentially converged within our formalism. Using this rate we have performed a study of the crust evolution of an accreting neutron star following the model of Ref. [1].

Our paper is organized as follows: The theoretical background is discussed in Sec. II, while Sec. III comments on the numerical strategies we have used to solve the HNC and respective Euler-Lagrange equations. The results of our study are presented and discussed in Sec. IV.

II. THE HYPERNETTED CHAIN APPROXIMATION

In the following, we will assume that the helium plasma is translationally invariant, isotropic, and homogeneous, and obeys Bose statistics. As we are interested in the plasma properties at very low temperatures ($T \leq 10^6$ K ≈ 86 eV), the system can be considered to be in its ground state. Then the many-body wave function is given by

$$\Psi(\{\mathbf{r}_1 \cdots \mathbf{r}_N\}) = \prod_{i<j} f^{(2)}(r_{ij}) \prod_{i<j<k} f^{(3)}(r_{ij}, r_{ik}, r_{jk}) \cdots , \tag{4}$$

where the $f^{(p)}$ describe p-body correlations in the wave function caused by the interaction among the constituents. All $f^{(p)}$ are real and positive, and, for radii larger than the range of the two-body forces, they asymptotically approach unity. (To simplify notation we drop the superscript on the two-body wave function and two-body correlation function throughout this paper.) The electrons present in the plasma will be treated as a homogeneous neutralizing background.

First we will restrict ourselves to two-body wave functions only, resulting in the Bijl-Dingle-Jastrow form of the many-body wave function, as given in Eq. (1).

Another central quantity in the description of homogeneous and isotropic quantum fluids is the radial correlation function. The two-body correlation function is defined as

$$g(\mathbf{r}_1, \mathbf{r}_2) = g(r_{12}) = \frac{N(N-1) \int d^3r_3 d^3r_4 \cdots d^3r_N \, |\Psi(\{\mathbf{r}_i\})|^2}{\rho^2 \int d^3r_1 d^3r_2 \cdots d^3r_N \, |\Psi(\{\mathbf{r}_i\})|^2} , \tag{5}$$

where N denotes the number of particles. It determines the relative probability to find particles i and j at a relative distance r_{ij}. Asymptotically $g(r)$ approaches unity. Its normalization follows from that of the many-body wave function (1):

$$\int dr^3 \, [g(r) - 1] = -1 . \tag{6}$$

In the hypernetted chain approximation, $g(r)$ is connected with $f(r)$ by a set of coupled nonlinear equations

$$g(r) = f^2(r) \exp\{N(r) + E(r)\} , \tag{7}$$

$$[1 - \rho\tilde{C}(k)]\tilde{N}(k) = \rho\tilde{C}(k)^2 , \tag{8}$$

$$C(r) = g(r) - 1 - N(r) , \tag{9}$$

where the tilde denotes the Fourier transform. $N(r)$ is the sum of the nodal diagrams

$$N(r_{12}) = \rho \int [g(r_{13}) - 1] \, [g(r_{23}) - 1 - N(r_{23})] \, d^3r_3 , \tag{10}$$

and $C(r)$ is called the sum of non-nodal diagrams. The basic elementary diagrams are usually classified in terms of the number of points n belonging to the diagram; for a definition the reader is referred to the review article by Zabolitzky [7]. To yield the exact $g(r)$ for a given $f(r)$, $E(r)$ has to be the infinite sum over all possible elementary diagrams. The approximative character of the various orders of HNC approximations reflects itself in the way $E(r)$ is replaced by a finite sum of diagrams:

$$E(r) = E_4(r) + E_5(r) + \cdots + E_n(r). \tag{11}$$

In the simplest approximation (HNC or HNC/0) one sets $E(r) = 0$. There is only one basic elementary diagram with four points:

$$E_4(r) = \frac{\rho^2}{2} \int d^3r_3 d^3r_4 [g(r_{13}) - 1][g(r_{14}) - 1][g(r_{23}) - 1][g(r_{24}) - 1][g(r_{34}) - 1] , \tag{12}$$

and there are seven diagrams with five points, which are shown in Fig. 1 using the standard conventions [7]. We will not consider elementary diagrams of higher order in this study. Equations (7)–(9) are called HNC/n equations where n refers to the level at which the expansion in Eq. (11) is truncated. The HNC/n scheme is physically reasonable [7], but it does not necessarily yield a converging series (see Refs. [8–11]). However, as a virtue of the optimal HNC approach, its breakdown by having no solution signals that new physics is required to describe the system. In many cases, the accuracy of the HNC/0 approximation is quite sufficient. [In the following, quantities calculated in the HNC/n approximation are distinguished by the subscript n. Again, to simplify notation, this index is dropped in HNC/4 approximation. Thus, $f(r)$ and $g(r)$ refer to the two-body wave function and correlation function calculated in the HNC/4 approximation.]

For reviews on the description of quantum fluids and the hypernetted chain approximation, we refer to

Refs. [8,12–14]. The first study of α-particle matter with Jastrow wave functions has been performed by Clark and Wang [15] (see also Refs. [16–18]). Our numerical treatment to solve the optimal HNC equations partly follows the work by Usmani *et al.* [19].

We will now derive at the Euler-Lagrange equations for our problem on the HNC/4 level. The Hamiltonian governing the many-body system is given by

$$H = \sum_i \frac{p_i^2}{2m_\alpha} + \sum_{i<j} [V_c(r_{ij}) + V_n(r_{ij})] + V_{\rm back} \ , \quad (13)$$

where the sums have to be taken over all ^{4}He nuclei present in the plasma. $V_c(r)$ describes the Coulomb interaction between two α particles, approximated by the one for two pointlike particles. $V_n(r)$ is the nuclear α-α potential for which we adopt

$$V_n(r) = \left[500 \exp\left\{-(0.7r)^2\right\} - 130.115 \exp\left\{-(0.475r)^2\right\}\right] \ \text{MeV}, \quad (14)$$

where r is measured in fm. This potential correctly describes the α-α phase shifts up to an energy of about 16 MeV [20]. We have slightly modified the depth parameter of the potential to additionally reproduce the ^{8}Be ground state as an s-wave resonance at $E_r = 92.12$ keV above the α-α threshold with a width of 6.8 eV.

The energy per particle is given by the Jackson-Feenberg form

$$\frac{E}{N} = \frac{\rho}{2} \int d^3r \left[g(r) \left(-\frac{\hbar^2}{4m_\alpha} \nabla^2 \ln f^2(r) + V_n(r) \right) + [g(r) - 1] V_c(r) \right] , \quad (15)$$

where the first integrand stems from the kinetic energy of the α particles, the second from their nuclear interaction, and the third takes care of the Coulomb interactions in the system of α particles and neutralizing electron background.

As $g(r)$ and $f(r)$ are related by the HNC/n equations, Eq. (15) can be interpreted as a functional of $f(r)$ or alternatively $g(r)$. Minimizing E_N with respect to $g(r)$ and using Eqs. (7)–(9), one derives the Euler-Lagrange equation for $g(r)$:

$$\left(-\frac{\hbar^2}{m_\alpha} \nabla^2 + V_c(r) + V_n(r) + W(r) \right) \sqrt{g(r)} = 0 \ . \quad (16)$$

m_α is the mass of the α particle, while $W(r)$ is the plasma-induced screening potential. It is convenient to split $W(r)$ into two parts: $W(r) = W_0(r) + W_e(r)$, where $W_0(r)$ is related to the liquid structure function $S(k) = 1 + \rho \widetilde{(g_0 - 1)}$ by

$$\tilde{W}_0(k) = -\frac{\hbar^2 k^2}{4m_\alpha \rho} \frac{[S(k) - 1]^2 [2S(k) + 1]}{S^2(k)} \ . \quad (17)$$

$W_e(r)$ considers the terms arising from the elementary diagrams. One has

$$W_e(r) = \frac{\hbar^2}{4m_\alpha} \left[\Delta E(r) + \int d^3r' g(r') \Delta' \frac{\delta E(r')}{\delta g(r)} \right] , \quad (18)$$

where Δ' indicates that the Laplace operator acts on the coordinate $\boldsymbol{r}'$. $\frac{\delta E(r')}{\delta g(r)}$ denotes the functional derivative of $E(r')$ with respect to $g(r)$.

To estimate the triple-α-fusion rate in the plasma, one has to determine the three-body correlation function $g^{(3)}$ at small separations. In HNC/n approximation, $g^{(3)}$ is related to the two-body correlation function by

$$g_n^{(3)}(r_{12}, r_{13}, r_{23}) = g_n^{(2)}(r_{12}) g_n^{(2)}(r_{13}) g_n^{(2)}(r_{23}) \exp\{A_n(r_{12}, r_{13}, r_{23})\} \ , \quad (19)$$

where the series of Abe diagrams

$$A = A_4 + A_5 + \cdots + A_n \quad (20)$$

has to be truncated consistently with the treatment of the elementary diagrams. In lowest order ($n = 0$) one has $A = 0$ and (19) becomes the simple Kirkwood approximation. The Abe diagrams relevant for $n = 4$ and $n = 5$ are shown in Fig. 2.

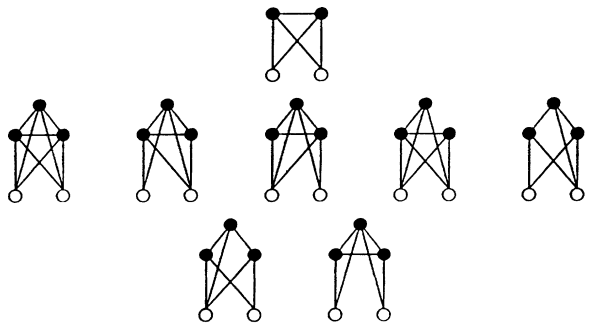

FIG. 1. The elementary diagrams with four [$E_4(r)$] (upper row) and five [$E_5(r)$] points (lower rows) using the convention as given in Ref. [7].

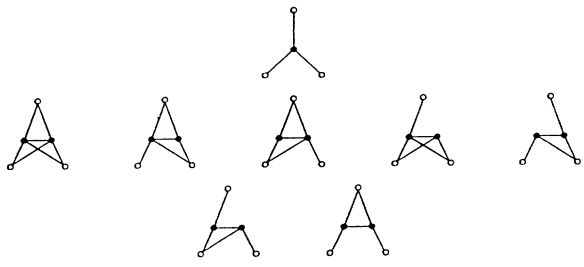

FIG. 2. The Abe diagrams with four (A_4) (upper row) and five (A_5) points (lower rows) using the convention as given in Ref. [7].

III. NUMERICAL STRATEGIES

The numerical solution of the problem stated in Sec. II is very involved. The HNC equations are a coupled set of nonlinear equations. Noticeably our problem involves two very different length scales: The Coulomb interaction requires a solution of the equations up to radii of about 1000 fm for the density region we are interested in, while a correct description of the nuclear α-α interaction including the ^{8}Be ground-state resonance requires a spatial resolution of ≈ 0.1 fm. An iterative treatment is necessary to solve the Euler-Lagrange equations, as the plasma-induced screening potential depends on the two-body correlation function itself. Finally, the calculation of the higher-order diagrams ($n > 0$) in either $E(r)$ and $A(r)$ involves multidimensional integrals.

Before we discuss how we have treated the various numerical challenges, we have to remark that a reliable solution of our problem requires an analytical treatment of the long-ranged correlations caused by the Coulomb interaction. For the HNC equations we followed here a procedure proposed in Ref. [21]. This method is based on the observation that the correlations in the plasma at large separations or small wave numbers are dominated by the plasma mode [22]. One finds [23]

$$S(k \to 0) = \frac{\hbar k^2}{\sqrt{64\pi e^2 \rho m_\alpha}} = \frac{\hbar k^2}{2 m_\alpha \omega_p} , \tag{21}$$

where $\omega_p = \sqrt{16\pi\rho e^2/m_\alpha}$ is the ion plasma frequency. With the help of the HNC equations, Eq. (21) translates into [2]

$$f(r \to \infty) \to \exp\left\{ -\frac{m_\alpha \omega_p}{4\pi\rho\hbar r} \right\} . \tag{22}$$

Defining

$$f^2(r) = \exp\{-u(r)\} \tag{23}$$

and splitting $u(r)$ into short- (u_s) and long-ranged (u_l) parts, one finds [21]

$$u_l(r) = \frac{\Gamma}{r}\left(1 - e^{-\beta r}\right) \tag{24}$$

with $\Gamma = (m_\alpha \omega_p)/(2\pi\hbar\rho)$; β is a free parameter. As $N(r) \sim \Gamma/r$ and $C(r) \sim -\Gamma/r$, one conveniently defines short-ranged functions

$$N_s(r) = N(r) - u_l(r), \tag{25}$$

$$C_s(r) = C(r) + u_l(r) , \tag{26}$$

which allow one to redefine the HNC equations by [21]

$$g(r) = \exp\{N_s(r) + E(r) - u_s(r)\} , \tag{27}$$

$$\tilde{N}_s(k) = \left(\rho \tilde{C}_s(k)\tilde{C}(k) - \tilde{u}_l(k)\right)[1 - \rho\tilde{C}(k)] , \tag{28}$$

$$C_s(r) = g(r) - 1 - N_s(r) . \tag{29}$$

In this derivation we have explicitly considered that $E(r)$ is short ranged. Equations (27)–(29) now state a short-ranged problem (the Fourier transform $\tilde{u}_l$ is analytically known [21]), which can be solved numerically after choosing a reasonable starting function for $g(r)$. The various Fourier transforms are most conveniently and efficiently done by fast-Fourier transform (FFT) routines [24].

As the plasma is overall neutral, the screening potential $W(r)$ has to exactly cancel the Coulomb interaction $V_c(r)$ in the Euler-Lagrange equations at large separations. For a numerical solution, this cancellation at large distances is essential and thus has to be guaranteed by an analytical treatment of the long-ranged components in $W(r)$. From Eqs. (17) and (21) one finds

$$\tilde{W}(k \to 0) = -\frac{16\pi e^2}{k^2} , \tag{30}$$

which translates into

$$W(r \to 0) = -\frac{4e^2}{r} . \tag{31}$$

To guarantee the cancellation of $W(r)$ and $V_c(r)$ at large distances, we define

$$\tilde{W}(k) = \left(\tilde{W}(k) - \tilde{W}_l(k)\right) + \tilde{W}_l(k) \tag{32}$$

$$= \tilde{W}_s(k) + \tilde{W}_l(k) \tag{33}$$

with

$$\tilde{W}_l(k) = -\frac{16\pi e^2}{k^2} \exp(-\alpha k) . \tag{34}$$

Its Fourier transform reads

$$W_l(r) = -\frac{4e^2}{r}\frac{2}{\pi} \operatorname{arc\,tan}\frac{r}{\alpha} , \tag{35}$$

which for large r approaches the desired asymptotic behavior (31). For the parameter α we adopted values of order 20 fm. While Eq. (35) guarantees the correct behavior of the screening potential at large r and an exact cancellation with the Coulomb potential, a numerical treatment of the short-ranged term $W_s(k)$ poses no problem and is conveniently done by using FFT routines.

We have solved the Euler-Lagrange equation using the Numerov algorithm with a step size of 0.1 fm. The problem was interpreted as an initial value problem with $rg(r) = 0$ at $r = 0$. At a sufficiently large distance the numerical solution and its derivative have been matched to their asymptotic forms in accord with Eq. (22).

Finally, our strategy to determine the optimal wave function $f(r)$ in HNC/4 approximation was as follows.

(1) First we have determined the optimal $f_0(r)$ following the procedure as outlined in Ref. [5]. This way we simultaneously calculated the corresponding $g_0(r)$.

(2) Using $g_0(r)$, we evaluated $E_4(r)$ by Monte Carlo integration. The result obtained was approximated by Gaussian functions (for a typical example, see Fig. 4 of Ref. [5]).

(3) $W(r)$ is calculated from Eqs. (17) and (18) where $E_4(r)$ is approximated by the analytical expression of step (2).

(4) The Euler-Lagrange (16) and HNC equations have been solved to obtain $g_4(r)$.

(5) Given the new two-body correlation function, steps (2)–(4) have been repeated until convergence has been achieved.

Note that convergence was usually achieved after one or two iteration steps, as then all calculated quantities agreed within the accuracy limitations in our procedure dictated by the Monte Carlo integration of $E_4(r)$ and the subsequent analytical approximation.

IV. RESULTS

A. Phase transition of the ^{4}He plasma

Schramm *et al.* were the first to point out that a helium plasma might undergo a phase transition to stable ^{8}Be matter at densities high enough to bind the ^{8}Be ground-state resonance by the plasma-induced screening potential [2]. This proposition has subsequently been confirmed in Ref. [6] based on an optimal HNC/0 approach. The critical density, at which the phase transition is expected to occur, has been estimated in the HNC/0 study to be about $\rho_{\rm cr} = 2.9 \times 10^9$ g/cm^3.

The present optimal HNC/4 approach confirms the proposed phase transition. However, the critical density is calculated to be somewhat larger ($\rho_{\rm cr} \approx 3.1 \times 10^9$ g/cm^3) due to repulsive contributions of $W_e(r)$ to the plasma-induced screening potential. The results of the optimal HNC/4 calculation are quantified in Figs. 3–5.

Figure 3 shows the plasma-induced screening potential. First, one observes that the screening potential in fact cancels the Coulomb potential at large distances. Second, we find that $W(r)$ has nearly a constant value $W(r) = E_{\rm sc}$ at small radii, say $r \leq 10$ fm. In Fig. 4 we have plotted these constant screening energies at small distances as a function of density. In a good approximation, $E_{\rm sc}$ obeys a simple power law:

$$E_{\rm sc} = -62.2 \times \rho_9^{1/3} \text{ keV} . \quad (36)$$

From Eq. (36) we recover that the screening energy equals the ^{8}Be ground-state resonance energy at $\rho \approx 3.2 \times 10^9$ g/cm^3. The density dependence of $E_{\rm sc}$ agrees with the power-law ansatz adopted by Fushiki and Lamb [4], who approximated the screening potential by the constant screening energy

$$E_{\rm sc} = -52.2 \times \rho_9^{1/3} \text{ keV} . \quad (37)$$

However, the screening potential $W(r)$ is not constant for all radii which are important for the barrier penetration process at the densities of interest here. While the approximation $W(r) = \bar{E}_{\rm sc}$ is roughly valid at the lower densities (e.g., in the density regime in which the triple-α rate plays an important role in the evolution of the neutron star crust, see below), it becomes noticeably worse at higher densities. Moreover, approximating $W(r)$ by a constant value can significantly fail, if the nuclear potential exhibits resonances, as in the present case. Replacing $W(r)$ by an average value $\bar{E}_{\rm sc}$ over the entire barrier penetration region results in $\bar{E}_{\rm sc} < E_{\rm sc}$ (e.g., in

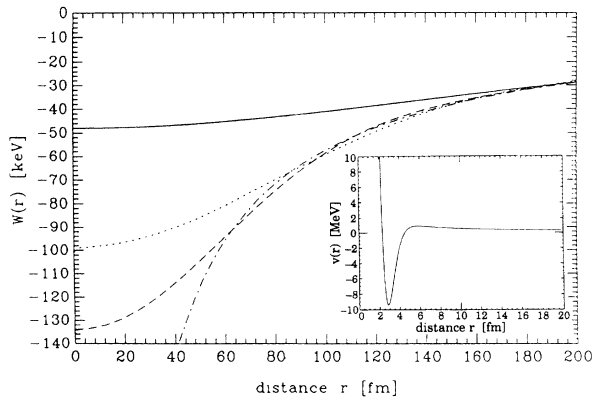

FIG. 3. The plasma-induced screening potential $W(r)$ is compared to the negative Coulomb potential $V_c = -4e^2/r$ (dash-dotted) at various densities: $\rho_9 = 0.5$ (solid), $\rho_9 = 4.0$ (dotted), and $\rho_9 = 10.0$ (dashed). The inset shows the potential $V(r) = V_c(r) + V_n(r)$ at nuclear separations.

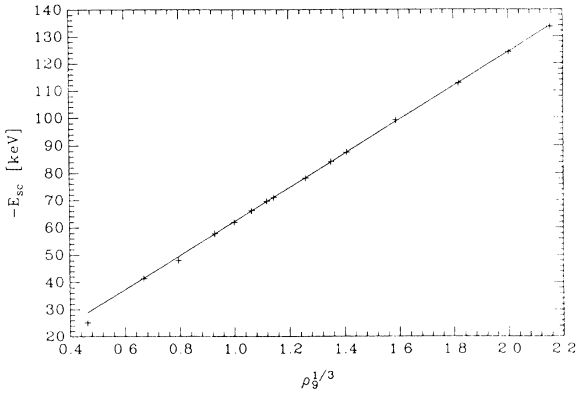

FIG. 4. The constant values of $W(r)$ at nuclear radii (*screening energies* $E_{\rm sc}$) as a function of density.

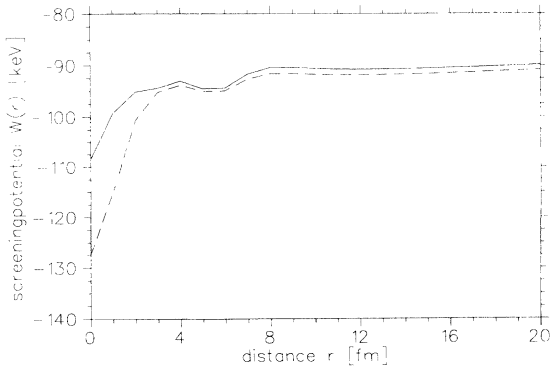

FIG. 5. The plasma-induced screening potential $W(r)$ (dashed line) and its $n = 0$ component $W_0(r)$ [Eq. (17), solid line] calculated at $\rho_9 = 3.2$, close to the critical density.

Refs. [4,2]), where E_{sc} is the value of the approximately constant screening potential at those small radii to which the resonance is mainly sensitive (36). Consequently, the influence of nuclear resonances will be shifted to higher densities if $W(r)$ is replaced by an average value $\bar{E}_{sc}$.

Deviating from the previous discussion, the screening potential calculated in the HNC/4 approximation is not constant at small radii at densities close to the critical density (Fig. 5). Comparing $W(r)$ with $W_0(r)$, we find that the contribution arising from the elementary diagram $E_4(r)$ smoothes out the short-ranged variations present in $W_0(r)$. Thus, the fact that close to the critical density the screening potential is not constant at small radii in the HNC/4 approach seems to indicate that in this density regime higher-order correlations beyond the $n = 4$ level are still important and will eventually compensate the fluctuations in $W(r)$. Unfortunately, a study of the helium plasma in the optimal HNC/5 approximation is beyond our numerical possibilities.

The phase transition from the helium plasma to stable ^{8}Be matter is again exemplified in Fig. 6, which shows the two-body correlation function $g(r)$ at three different densities, $\rho_9 = 0.5$, 3.2, and 10.0. For comparison, this figure also shows $g(r)$ calculated without consideration of the nuclear α-α potential. In this case, the results for the familiar charged Bose liquid, as published in Ref. [21], are recovered. As a striking difference, the two-body correlation functions calculated in the present HNC/4 approach exhibit pronounced maxima at around $r = 3.1$ fm, which are missing in the charged Bose liquid case. Obviously, these correlations are caused by the short-ranged attractive α-α potential. Comparing $g(r)$ at different densities, one finds that at $\rho_9 = 0.5$ the magnitude of the correlations induced by the α-α potential at nuclear radii is smaller than the long-ranged Coulomb-induced correlations by several orders of magnitude. At these densities, which are of importance for the evolution of the neutron star crust, the helium liquid is still dominated by long-ranged Coulomb order. The situation is clearly different at $\rho_9 = 3.2$, close to the critical density. Here, the short-ranged correlations are noticeably larger than the Coulomb-induced ones; the helium plasma prefers the ^{8}Be-like structure. At higher densities, for example $\rho_9 = 10$, the helium plasma still shows strong correlations at nuclear radii. However, their magnitudes are noticeably less pronounced than in the vicinity of the critical density due to increasing Coulomb repulsion.

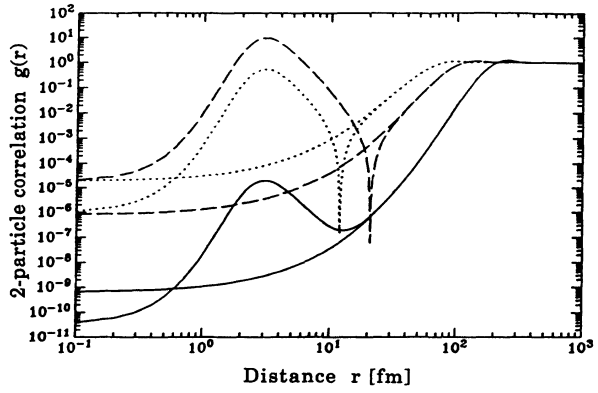

FIG. 6. The two-particle distribution function in optimal HNC/4 approximation for the charged Bose liquid (without maximum at $r = 3.1$ fm) and for the helium plasma, calculated at different densities: $\rho_9 = 0.5$ (solid), $\rho_9 = 3.2$ (dashed), and $\rho_9 = 10.0$ (dotted).

Table I lists the total energy and its various contributions for several densities in the range $\rho_9 = 0.1$–10.0. While the Coulomb energy monotonously decreases with density, as expected, the nuclear energy has a pronounced minimum at the critical density. However, even in the vicinity of the critical density, the Coulomb energy contributes the largest part to the total energy, which, in absolute value, is found to be monotonously increasing with ρ for the range of densities studied in this paper.

We would like to close this subsection with two remarks concerning the applicability of the HNC approximation to helium plasma at densities higher than the critical density.

(1) The phase transition actually described in the HNC approach corresponds to one from a helium plasma to a ^{8}Be plasma (the situation is sketched in Fig. 7). However, at $\rho \approx \rho_{cr}$, ^{8}Be matter will exist in the form of a Wigner-Seitz crystal rather than a quantum liquid, as modeled in the HNC approach. Assuming ^{8}Be matter to exist as a Coulomb lattice with fcc structure, the critical density is lowered to about $\rho_{cr} = 2.3 \times 10^9$ g/cm^3 [2].

(2) As a striking feature, the correlation function $g(r)$ exhibits sharp minima at around $r = 20$ fm for $\rho > \rho_{cr}$ (Fig. 6). These minima are related to a node in the wave function $f(r)$ introduced by the requirement of orthogonality on the ^{8}Be ground-state resonance posed by the Schrödinger-like Euler-Lagrange equation. As the ground-state wave function of a Bose system is nodeless, the HNC approach does not describe the ground state of the helium plasma at $\rho > \rho_{cr}$. As we have discussed above, the physical ground state should correspond to a Coulomb lattice of ^{8}Be matter.

TABLE I. Kinetic energy (T), Coulomb energy (E_{Coul}), nuclear energy (E_{nucl}), and total energy (E_{tot}) for a helium plasma at various densities, as calculated in optimal HNC/4 approximation. All energies are in keV and per particle.

ρ_9	T	E_{Coul}	E_{nucl}	E_{tot}
0.1	0.964	−18.71	-1.19×10^{-11}	−17.75
0.3	1.649	−26.77	-5.23×10^{-8}	−25.12
0.5	2.093	−31.52	-1.06×10^{-6}	−29.42
0.8	2.525	−36.58	-2.42×10^{-5}	−34.06
1.2	3.015	−41.61	-3.06×10^{-4}	−38.59
1.5	3.328	−44.66	-1.34×10^{-3}	−41.33
2.0	3.780	−48.91	-1.13×10^{-3}	−45.14
2.5	4.224	−52.46	-9.86×10^{-2}	−48.33
3.0	4.839	−55.38	-5.48×10^{-1}	−50.11
3.1	6.806	−54.73	−3.676	−51.60
3.2	6.660	−55.44	−3.326	−52.10
3.4	5.917	−56.87	−2.036	−52.99
4.0	5.527	−60.56	-7.36×10^{-1}	−55.76
6.0	6.283	−68.96	-3.70×10^{-1}	−63.05
10.0	7.900	−80.85	-5.69×10^{-1}	−73.52

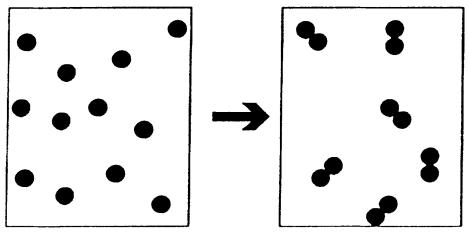

FIG. 7. Schematic sketch of the phase transition in the helium plasma within the HNC approach.

B. The triple-α-fusion rate

According to the model by Blaes *et al.* [1], the triple-α-fusion rate plays a decisive role in the crust evolution of an old accreting neutron star. For this problem, the rate has to be known in the density regime from 10^8 g/cm^3 to a few 10^9 g/cm^3. Using the definition, as given by Eq. (3) in the Introduction, we have calculated the triple-α rate in the optimal HNC/4 approximation.

The authors of Ref. [5] have studied the influence of higher-order HNC/n corrections on the triple-α rate. It was found that for a given wave function (in Ref. [5] this was the optimal wave function in HNC/0 approximation), the triple-α rate converged with higher corrections ($n = 4, 5$). A reasonable limit is already obtained if $g^{(3)}(r)$ is consistently calculated on the HNC/5 level. Thus, following our previous work [5], we have considered the $n = 5$ corrections in the two-body correlation function. To achieve this goal, we have solved the HNC equations in the $n = 5$ approximation for the optimal HNC/4 wave function. The elementary diagrams $E_5(r)$ have been calculated numerically by Monte Carlo integration and were then approximated by Gaussians. Consistently with this procedure, the three-body correlation function $g^{(3)}$, required in the estimate of the triple-α rate, has also been calculated in fifth order, replacing $A(r)$ in Eq. (19) by $A(r) = A_4 + A_5$. The integrals have been evaluated by Monte Carlo techniques. Equation (3) requires the average of the rate over the nuclear reaction volume, which we have approximated by a sphere of radius 5 fm. Note that the Abe diagrams are found to be nearly constant for the radial parameters corresponding to the reaction volume (see Fig. 8 in Ref. [5]).

Our calculated triple-α rate is shown in Fig. 8. The $n = 5$ corrections are found to change the rates only slightly. Under neutron star conditions the triple-α process is expected to occur most effectively at $\rho_9 \approx 0.5 - 1$ [1]. At these densities, the rates calculated in optimal HNC/0 and HNC/4 approximations [both with ($n = 5$) corrections] nearly coincide. Here, the HNC results also agree reasonably well (within 30%) with the estimates from Fushiki and Lamb [4], calculated within a coupled-channel S-matrix approach using a WKB approximation for the particle tunneling amplitude. However, in this approach [4] the resonant enhancement of the rate, associated with the ^{8}Be ground state, concentrates at around $\rho_9 \approx 5$, which is noticeably higher than found in the HNC calculations. We believe that this difference is caused by

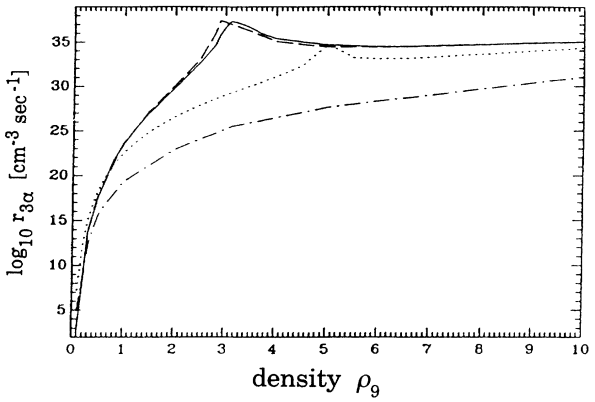

FIG. 8. The pycnonuclear triple-alpha-fusion rates calculated in various levels of HNC approximation: optimal HNC/4 with ($n = 5$) corrections (solid curve), optimal HNC/0 with ($n = 5$) corrections (dashed curve). The present results are compared to those of Fushiki and Lamb [4] (dotted curve) and of Cameron [3] (dash-dotted curve).

the assumption of a constant screening energy in Ref. [4], which is smaller than the plasma-induced screening potential $W(r)$ in the HNC calculations at those small radii at which the ^{8}Be ground-state resonance forms. All rates, including the one of Ref. [2] which agrees with the estimate of Fushiki and Lamb for $\rho_9 < 1$, are noticeably higher than the original one by Cameron [3].

Following Ref. [3] we find that our rates (in cm^{-3} s^{-1}) obtained in optimal HNC/4 approximation with $n = 5$ corrections are well reproduced by

$$\ln r_{3\alpha} = 3 \ln \rho_9 - 91.23 \rho_9^{-1/6} + 146.56 \, . \qquad (38)$$

This is exemplified in Fig. 9. The deviation from this simple parametrization for $\rho_9 \geq 2$ is caused by the increasing influence of the ^{8}Be resonance.

Adopting the model by Blaes *et al.* [1], we have studied the evolution of a neutron star crust after hydrogen fusion. For the triple-α rate we used the parametrization (38). We find that helium fusion stops with the production of oxygen (Fig. 10), as essentially no helium is left

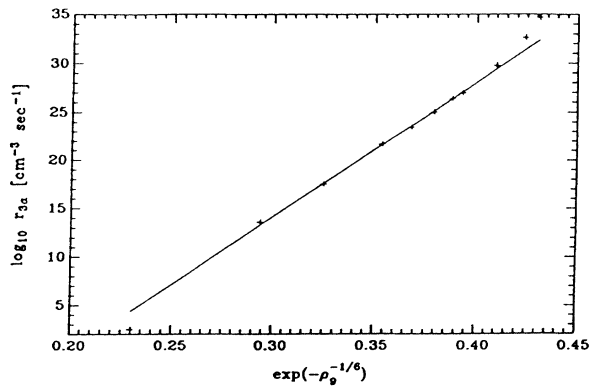

FIG. 9. The density dependence of the reaction rate in the nonresonant density region.

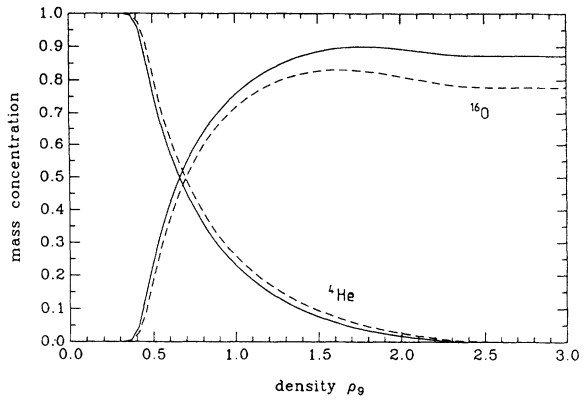

FIG. 10. Pycnonuclear evolution of the accreted layer on the neutron star after hydrogen burning, adopting the model of Ref. [1]. The diagram shows the mass concentration of the dominating elements as a function of density calculated with the present pycnonuclear triple-alpha rate (solid) and the one of Ref. [4] (dashed).

over after the fast triple-α reaction to allow for helium fusion processes beyond oxygen. The same conclusions are reached if the rate of Fushiki and Lamb is adopted (Fig. 10 and Ref. [1]). Thus, our rate supports the star-quake scenario proposed by Blaes *et al.*, where the freshly formed oxygen will eventually undergo a two-stage electron capture to ^{16}C, which then is followed by a density turnover at the interface of the freshly evolved ^{16}C with the crust of the old neutron star, triggered by Rayleigh-Taylor instabilities.

C. Three-body correlations in the wave function

We have tried to improve our description of the helium plasma by additionally considering three-particle terms in the many-body wave function (4). Following Ref. [25] we made the following ansatz:

$$f^{(3)}(r_{ij},r_{ik},r_{jk}) = \exp\left(-\frac{1}{2}q(r_{ij},r_{ik},r_{jk})\right) \tag{39}$$

with

$$q(r_{ij},r_{ik},r_{jk}) = \sum_{\text{cyc}} \chi(r_{ij})\chi(r_{ik}) \tag{40}$$

and

$$\chi(r) = a\cdot(r-r_t)\cdot\exp\left(-\left(\frac{r-r_t}{\omega}\right)^2\right) . \tag{41}$$

a, r_t, and ω are interpreted as variational parameters. Our strategy was to determine these parameters by minimizing the energy of the system

$$\frac{E}{N} = \frac{\rho}{2}\int d^3r\left[g(r)\left(-\frac{\hbar^2}{4m_\alpha}\nabla^2\ln f^2(r)+V_n(r)\right)+[g(r)-1]V_c(r)\right] + \frac{\hbar^2}{16m_\alpha}\rho^2\int d^3r_{ij}d^3r_{ik}g^{(3)}(r_{ij},r_{ik},r_{jk})\nabla_i^2 q(r_{ij},r_{ik},r_{jk}) \tag{42}$$

subject to the condition that $f(r)$ is given by the optimal two-body wave function determined in HNC/4 approximation. The three-body correlation function can be expressed as

$$g_4^{(3)}(r_{12},r_{13},r_{23}) = g^{(2)}(r_{12})g^{(2)}(r_{13})g^{(2)}(r_{23})f^{(3)}(r_{12},r_{13},r_{23})\exp\{A_4(r_{12},r_{13},r_{23})\} , \tag{43}$$

where the Abe diagrams now also contain three-particle contributions [25]. Similarly, the elementary diagrams have to be extended to account also for three-particle terms; i.e., there are eight additional diagrams contributing to $E_4(r)$ [25]. Finally, the HNC equations are modified to

$$g(r) = f^2(r)\exp\{N(r)+D(r)+E(r)\} , \tag{44}$$

$$N(r_{12}) = \rho\int[g(r_{23})-1]\,[g(r_{13})-1-N(r_{13})]\,d^3r_3 , \tag{45}$$

$$D(r_{12}) = \rho\int\left[(f^{(3)})^2(r_{12},r_{13},r_{23})-1\right]\,g(r_{13})g(r_{23})\,d^3r_3 . \tag{46}$$

Note that the integrals appearing in Eqs. (44)–(46) exhibit more structure than those in $E_4(r)$ and $E_5(r)$ on the two-particle level discussed above. Thus, the analytical approximation of these integrals by Gaussians is more involved and probably also less accurate than for the two-body case.

In Table II we compare the ground-state energy of the charged Bose liquid, as calculated in the optimal HNC/4 approximation, with the results of a presumably exact Monte Carlo approach [26]. One observes that the two-body ansatz on the HNC/4 level already reproduces the exact results within 1% for the densities of interest here. Thus, we expect that the consideration of three-body correlations in our description of the helium plasma is likely to improve on the short-ranged nuclear correlations rather than on the long-ranged Coulomb-induced correlations. We have therefore restricted our study of the helium plasma to the parameter space $0 < a \leq 1$, $0 \leq r_t \leq 50$ fm, and $0 < \omega \leq 50$ fm. The density was first chosen as $\rho_9 = 3.2$, as it seems more likely that

TABLE II. Comparison of the ground-state energies (in keV and per particle) of the charged Bose liquid calculated in optimal HNC/4 approximation ($E_{\mathrm{HNC/4}}$) and in an exact Monte Carlo approach (E_{exact} [26]).

ρ_9	$E_{\mathrm{HNC/4}}$	E_{exact}
0.268	−24.21	−24.50
2.147	−46.12	−46.49
33.55	−105.30	−105.86
268.4	−192.31	−192.96
2147.0	−343.58	−344.05

three-body correlations play a role in the phase transition regime than at those densities at which the helium plasma is dominated by Coulomb order.

Systematically varying the parameters in the space defined above, we were not able to improve the total energy of the system beyond the accuracy of our calculation, which we estimate to be about four digits in E/N. We find several solutions (different regions in parameter space) which result in the same total energy, but differ in their estimates for the partial contributions to the energy (kinetic, nuclear, Coulomb). Relatedly, these solutions predict different two-body and three-body correlations at nuclear separations. This allows us to estimate the uncertainty in the triple-α rate by studying its variation over all solutions with the same (within our numerical accuracy) total energy. This way, we find that at $\rho_9 = 3.2$ the rate fluctuates between one-tenth and twice the value obtained in the optimal HNC/4 approach (Sec. IV B) for the parameter space defined above. Repeating our study at $\rho_9 = 4.0$, we observe similar uncertainties. For $\rho_9 < 1$, which is the density regime of relevance for the crust evolution of an old neutron star, a similar estimate of the uncertainties in the rates is prohibited, as the nuclear contributions to the total energy are too small to be reliably controlled within the accuracy of our calculation (see Table I). As at these densities the helium plasma is strongly Coulomb dominated, it is likely that three-body correlations are less important than at densities close to the phase transition. Thus, the relative uncertainty of the triple-α rate, as estimated at $\rho_9 = 3.2$ and 4.0, might be taken as a conservative limit for $\rho_9 < 1$. With this assumption, the triple-α rate in the helium plasma is always fast enough to support the scenario in the starquake model of Blaes *et al.* [1], which leads to the ^{16}C/^{56}Ti interface and an energy release comparable to the one observed in γ-ray bursts [1].

Finally, we would like to remark that the short-ranged correlations in the helium plasma at densities close to the critical density can be studied in an exact Monte Carlo approach similar to the one performed by Ceperley for the charged Bose liquid [26]. In our opinion, such a study is desirable as it would answer the question raised by the present HNC calculation whether higher correlations are important to describe the helium plasma at these densities. In contrast, an exact Monte Carlo calculation cannot be used to determine the triple-α rate at $\rho_9 < 1$, as the relative probability to find three α particles very close together in a helium plasma at these densities is too small to sample the rate with reasonable statistics within an acceptable computer time. However, for its application in the crust evolution of an old, accreting neutron star, we believe that the rate is probably determined accurately enough from our HNC calculations.

ACKNOWLEDGMENTS

We thank S. E. Koonin and S. Schramm for many helpful discussions. We are also indebted to O. Blaes for providing us with his neutron star surface evolution code. This work was supported in part by the National Science Foundation Grant Nos. PHY90-13248 and PHY91-15574.

[1] O. Blaes, R. Blandford, P. Madau, and S. E. Koonin, Astrophys. J. **363**, 612 (1990).
[2] S. Schramm, K. Langanke, and S. E. Koonin, Astrophys. J. **397**, 579 (1992).
[3] A. G. W. Cameron, Astrophys. J. **130**, 916 (1959).
[4] I. Fushiki and D. Q. Lamb, Astrophys. J. **317**, 368 (1987).
[5] H.-M. Müller and K. Langanke, Z. Phys. A **342**, 133 (1992).
[6] K. Langanke, D. Lukas, H.-M. Müller, S. Schramm, and S. E. Koonin, Z. Phys. A **339**, 419 (1991).
[7] J. G. Zabolitzky, in *Advances in Nuclear Physics*, edited by J. W. Negele and E. Vogt (Plenum Press, New York, 1981), Vol. 12, p. 1.
[8] E. Feenberg, *Theory of Quantum Fluids* (Academic Press, New York, 1969).
[9] E. Krotscheck, Phys. Rev. A **15**, 397 (1977).
[10] E. Krotscheck, Nucl. Phys. **A293**, 293 (1977).
[11] A. D. Jackson, A. Lande, and L. J. Lantto, Nucl. Phys. **A317**, 70 (1979).
[12] C. W. Woo, in *The Physics of Liquid and Solid Helium*, edited by K. H. Bennemann and J. B. Ketterson (Wiley, New York, 1976).
[13] C. E. Campbell, in *Progress in Liquid Physics*, edited by C. A. Croxton (Wiley, New York, 1978), Chap. 6.
[14] J. W. Clark, Prog. Part. Nucl. Phys. **2**, 89 (1979).
[15] J. W. Clark and T. P. Wang, Ann. Phys. (N.Y.) **40**, 127 (1966).
[16] M. Harada, R. Tamagaki, and H. Tanaka, Prog. Theor. Phys. **29**, 933 (1963).
[17] G. P. Mueller and J. W. Clark, Nucl. Phys. **A155**, 561 (1970).
[18] M. T. Johnson and J. W. Clark, Kinam **2**, 3 (1980).
[19] Q. N. Usmani, B. Friedman, and V. R. Pandharipande, Phys. Rev. B **21**, 4502 (1982).
[20] S. Ali and A. R. Bodmer, Nucl. Phys. **80**, 99 (1966).
[21] J. F. Springer, M. A. Prokrant, and F. A. Stevens, J. Chem Phys. **58**, 4863 (1973).
[22] D. Pines and Ph. Noizières, *The Theory of Quantum Liquids* (W. A. Benjamin, New York, 1966).
[23] L. J. Lantto and P. J. Siemens, Nucl. Phys. **A317**, 55 (1979).
[24] W. H. Press, B. P. Flannery, S. A. Teukolsky, and W. T. Vetterling, *Numerical Recipes* (Cambridge University Press, Cambridge, 1986).
[25] Q. N. Usmani, S. Fantoni, and V. R. Pandharipande, Phys. Rev. B **26**, 6123 (1982).
[26] D. M. Ceperley and B. J. Alder, Phys. Rev. Lett. **45**, 566 (1980).